

Multi-Phase EMTR-based Fault Location Method Using Direct Convolution Considering Frequency-Dependent Parameters and Lossy Ground

Guanbo Wang, Chijie Zhuang, *Member, IEEE*

Abstract—Many Electromagnetic time reversal (EMTR)-based fault location methods were proposed in the latest decade. In this paper, we briefly review the EMTR-based fault location method using direct convolution (EMTR-conv) and generalize it to multi-phase transmission lines. Moreover, noting that the parameters of real transmission lines are frequency-dependent, while constant-parameters were often used during the reverse process of EMTR-based methods in the previous studies, we investigate the influence of this simplification to the fault location performance by considering frequency-dependent parameters and lossy ground in the forward process which shows the location error increases as the distance between the observation point and the fault position increases, especially when the ground resistivity is high. Therefore, we propose a correction method to reduce the location error by using double observation points. Numerical experiments are carried out in a 3-phase 300-km transmission line considering different ground resistivities, fault types and fault conditions, which shows the method gives good location errors and works efficiently via direct convolution of the signals collected from the fault and the pre-stored calculated transient signals.

Index terms—Electromagnetic Time Reversal, fault location, direct convolution, frequency-dependent transmission line, lossy ground

I. INTRODUCTION

As the power system capacity increases, quick and accurate short-circuit fault location becomes more and more important for continuous and safe power supply.

Existing fault location methods can mainly be divided into two categories: impedance-based [1][2] and traveling wave-based [3]-[6]. The impedance-based methods are straightforward; however, its accuracy is easily affected by the fault impedance and network structure. Traveling wave-based methods have better accuracy but require high-frequency signal acquisition equipment, and therefore more cost. In the last decades, a new type of traveling wave-based fault location methods, namely, Electromagnetic Time Reversal (EMTR)-based methods, has been proposed, and gained extensive research interest [7-10]. Compared with traditional traveling wave-based methods, it is reported in [11] that EMTR-based methods are able to work under lower sampling rates (i.e., 100 kS/s), resulting in a lower cost.

In this paper, we focus on the EMTR-based methods. The EMTR method was applied to transmission line fault location in 2012 [7], since then lots of studies on the practicability of these methods have been conducted by numerical simulations and real experiments [8-13]. A test in a complex T-network composed of a single cable and cables with different wave impedances was numerically carried out in [8], which shows that the accurate location of short-circuit faults only requires a signal measurement at one end. Moreover, the line loss is considered in [9]-[10] using constant line parameters, which shows that the line loss has little influence on the fault

location accuracy for transmission lines with a length of less than, e.g., 50 km. Meanwhile, experiments on EMTR fault location methods have been carried out. Wang et al. conducted fault location experiments in medium voltage distribution networks both in China and Switzerland respectively [12][13], which show that the fault locations can be correctly identified; however, these experiments were carried in small-scale power networks, e.g., using lines less than several-km long.

In general, the EMTR-based fault location process can be divided into two stages: the forward and the reverse process. During the forward process, fault-generated transient signals are collected or measured at one or two ends of the transmission line. During the reverse process, a series of assumed short-circuit branches are set along the transmission line as the guess fault locations (GFLs), and the transient signals are injected back to the transmission line after time reversal; the fault current signal energies (FCSEs) are numerically calculated, and the position where the maximum of the FCSEs is achieved is the real fault position.

We wish to emphasize that, in real applications, during the forward process, the fault generated transient signals propagate through real power lines and then be measured. The power line parameters are frequency-dependent and influenced by the lossy ground. However, in the reverse process, FCSEs are often calculated using constant or averaged parameters, e.g., in [7]-[13]. Using constant line parameters in simulations is also the case in many existing literatures on fault location methods [14-17]. An accurate wave velocity is crucial to locate the faults for the traveling wave-based methods. However, in real applications, the wave propagation velocity (or transmission line parameters) is measured under a certain frequency. Therefore, it is not common to consider the frequency-dependent wave velocity, and constant parameters are widely used. For short lines, this may not be a big problem, as shown in [8][12] and [13]. It is worth noting that in [12] and [13], the lines are relatively short and the ground resistivity is low, e.g., the transmission line in [12] is totally 677-meter-long and the ground resistivity is 10 Ωm ; the fault distance in [13] is less than 3.6 km, therefore the influence wasn't clearly observed. However, for long transmission lines, we may expect that the location error grows due to the frequency dependency of the wave velocity, which will be shown later.

The second motivation of this work is that in the reverse processes, the FCSEs are calculated repeatedly for each guessed fault location, resulting in repeated calls to electromagnetic transient simulation software. In [18], a new EMTR-based fault location method using direct convolution (EMTR-conv) was proposed, which only requires the pre-calculation of assumed transients at the GFLs once for a given network, and can be used repeatedly for multiple faults. The

derivation and numerical experiments of EMTR-conv were carried out using single transmission lines, while the effectiveness of the method in multi-phase transmission lines needs validation.

The main contribution of the paper includes:

- (1) We generalize the EMTR-conv method, which only requires a direct convolution of the measured transient signal and a pre-computed signal, to multi-phase transmission line fault locations.
- (2) We consider the influence of frequency-dependent line parameters and lossy ground to the location accuracy, especially for relatively long transmission lines in areas with high ground resistivity; and propose an effective formula to correct the location error. By using this formula, it is safe to use frequency-independent constant line parameters (wave velocity) in the reverse process.

The rest of the paper is organized as follows: in section II, the EMTR-based fault location method using direct convolution (EMTR-conv) is briefly reviewed; in section III, EMTR-conv method is extended to multi-phase lines for different types of faults; section IV considers the influence of frequency-dependent parameters and lossy ground: when constant-parameter lines are used in the reverse process, the location error grows roughly proportional to the fault distance, and a correction method is proposed accordingly. An application to a 300-km real transmission line under different fault conditions is given in section V. Finally, some conclusions are drawn in section VI.

II. EMTR FAULT LOCATION METHOD USING DIRECT CONVOLUTION (EMTR-CONV): SINGLE PHASE LINE CASES

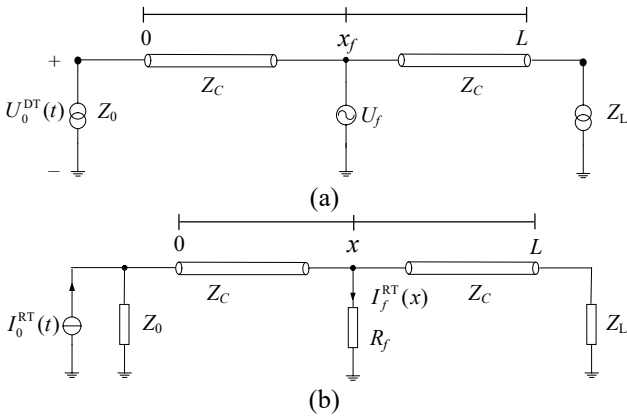


Fig. 1. Representation of a fault along a single-conductor transmission line (forward process) and the reverse process.

The principle of the classical EMTR fault location method has been given in a series of papers [7]-[13]. Though there exist other variants, we focus on one of the most classical ones, and use a single conductor case for example to illustrate the main principle, because the principle remains similar.

Fig. 1(a) shows the forward process (or in the *direct time*, DT), a short-circuit fault occurs at $x = x_f$, which is represented by a voltage source U_f . Z_0 and Z_L are the input impedances of the transformers. The frequency spectrum for fault-originated transients is usually up to hundreds of kilohertz, therefore the input impedance generally behaves like a capacitance of several hundreds of pF [8], and is equivalent to a large impedance. The high frequency components of the transient can hardly pass through the

transformers and interact with the source or load. So the source impedance and load are not taken into consideration, and we only need to focus on the propagation and reflection between both ends. Z_C is the surge impedance of transmission lines. As in [18], the transient at one end of the line in the frequency domain $U_0^{DT}(\omega)$ is

$$U_0^{DT}(\omega) = \frac{(1 + \rho_0)e^{-\gamma x_f}}{1 + \rho_0 e^{-2\gamma x_f}} U_f(\omega), \quad (1)$$

where $\gamma = j\beta = j\omega/v$ for lossless conductor, v is the propagation speed and ρ_0 is the voltage reflection coefficient,

$$\rho_0 = \frac{Z_0 - Z_C}{Z_0 + Z_C}. \quad (2)$$

In the reverse process (or in the *reversed time*, RT), the signal is re-injected into the original system from the same end after the time reversal operation and Norton equivalent as shown in Fig. 1(b).

$$I_0^{RT}(\omega) = \frac{[U_0^{DT}(\omega)]^*}{Z_0}. \quad (3)$$

A series of priori assumed short-circuit branches are set along the line as the guessed fault locations (GFLs). Neglecting the fault impedance, the corresponding short-circuit current is

$$I_f^{RT}(x, \omega) = \frac{(1 + \rho_0)^2 e^{-\gamma(x-x_f)}}{(1 + \rho_0 e^{-2\gamma x})(1 + \rho_0 e^{2\gamma x_f})} U_f^*(\omega). \quad (4)$$

The fault current signal energy (FCSE) reaches the maximum when $x_f' = x_f$, therefore the fault can be located by calculating the fault current at different GFLs and finding the maximal FCSE.

From Eq. (4), we note that the maximum point of FCSE is irrelevant to the energy-bounded signal $U_f(\omega)$, if we replace the time-reversed signal $I_0^{RT}(\omega)$ with an arbitrary energy-bounded signal $U(\omega)$ (i.e., $0 < \int_{-\infty}^{+\infty} |U(\omega)|^2 d\omega < +\infty$), the fault current is

$$I_f^{RT}(x, \omega) = \frac{(1 + \rho_0)e^{-\gamma x}}{Z_0(1 + \rho_0 e^{-2\gamma x})} U(\omega). \quad (5)$$

The convolution of (1) and (5) is therefore

$$C(x, \omega) = I_f^{RT}(x, \omega) U_0^{DT}(\omega) = \frac{(1 + \rho_0)^2 e^{-\gamma(x_f+x)}}{Z_0(1 + \rho_0 e^{-2\gamma x_f})(1 + \rho_0 e^{-2\gamma x})} U_f(\omega) U(\omega). \quad (6)$$

Note that the magnitude of the convoluted signal (6) will have the same structure as (4), we may expect that the convoluted signal energy (CSE) also reaches the maximum at $x = x_f$ unaffected by the choice of $U(\omega)$, which indicates that we can inject an (almost arbitrary) signal in the reverse process to accomplish the fault location [18]. Therefore, an EMTR-based fault location method using direct convolution (EMTR-conv) (as well as Eqs. (1) to (5)) is proposed in [18]:

- (1) [reverse process] For a given network, we can set a series of guessed short-circuit branches along the line as the GFLs, and calculate the transient at the GFLs under an arbitrary excitation source at one end of the line. The results are then stored. This can be done before a real fault occurs.
- (2) [forward process] When a real fault occurs, the fault-generated transient signal is collected at the same end of the line in (1).
- (3) The transient signal collected in (2) is convoluted with each pre-stored transient at the GFLs. The CSE of each convoluted signal is calculated, and the maximal CSE corresponds to the real fault position.

Numerical experiments were carried out in a 20-km single-phase line to validate the EMTR-conv algorithm. PSCAD/EMTDC with a time step of $0.1 \mu\text{s}$ was used to generate the transient, and MATLAB was used in the simulations to implement the convolution. However, the convolution can be done in embedded hardware instead in real applications.

The parameters of the power line are shown in Table I. $100\text{-k}\Omega$ large resistances are used to represent the power transformers at both ends of the line. Short-circuit faults with an impedance of 1Ω are set along the line respectively and the fault-generated transient voltage signals at one end of the line are obtained respectively in the forward process. In the reverse process, short-circuit branches with a $1\text{-}\Omega$ fault resistance are set along the line at every guessed fault location. The short-circuit currents at different GFLs under the excitation of a lightning impulse

$$u(t) = 10(e^{-t/\alpha} - e^{-t/\beta}) \text{ kV}, \alpha = 20 \mu\text{s}, \beta = 3 \mu\text{s} \quad (7)$$

at the same end of the line are then calculated, respectively. The signals re-injected into the original system (Eq. (6)) is not necessarily the time-reversed transient signal (Eq. (3)), which is a fundamental difference from the original EMTR-based methods.

We remark that although we use the transmission line parameters in the simulations, but what EMTR-based methods require is the wave velocity of the transient. By changing the transmission line parameters but keeping the wave velocity unchanged, the location results remain the same. This can be understood from the telegraph equations which describes the wave propagation.

TABLE I. SINGLE-PHASE TRANSMISSION LINE PARAMETERS

Parameter	Value
Length	20 km
Inductance	$1.6 \mu\text{H/m}$
Capacitance	10.54 pF/m
DC resistance	$0.036 \Omega/\text{km}$

The CSEs for different real and guessed fault locations are shown in Fig. 2, and the CSEs are normalized by all divided by the maximum energy. The maximum points of the CSE always appear at the real fault position as is shown in Fig. 2, which illustrates the correctness of the method.

Interested readers may refer to [18] for more details.

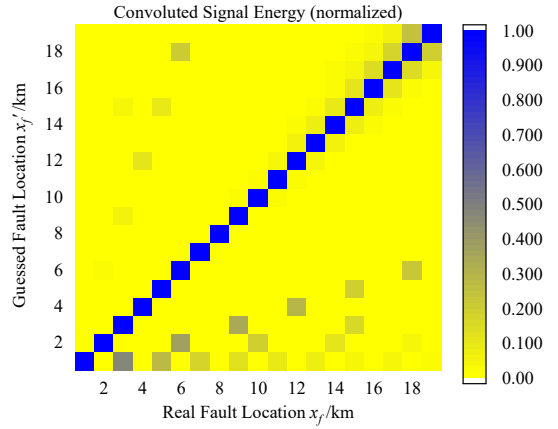


Fig. 2. The convoluted signal energy at different GFLs. The fault was simulated using Bergeron models with a time step of $0.1 \mu\text{s}$ and the signal length used to do the convolution was 5 ms .

Though the rigorous theoretical proof on this method needs further investigation, we give a consideration on why it works.

The transfer functions of the forward and reverse process are

$$H^{\text{DT}}(\omega) = \frac{U_0^{\text{DT}}(\omega)}{U_f(\omega)} = \frac{(1 + \rho_0)e^{-\gamma x_f}}{1 + \rho_0 e^{-2\gamma x_f}}, \quad (8)$$

$$H^{\text{RT}}(x, \omega) = \frac{I_f^{\text{RT}}(x, \omega)}{I_0^{\text{RT}}(\omega)} = \frac{(1 + \rho_0)e^{-\gamma x}}{1 + \rho_0 e^{-2\gamma x}}. \quad (9)$$

Wang et al. studied the transfer functions Eq. (8) and (9) [19] and found the magnitude of $H^{\text{DT}}(\omega)$ reaches the local maximum when

$$f_k^{\text{DT}} = (2k + 1) \frac{v}{4x_f}, k = 0, 1, 2, \dots \quad (10)$$

Similarly, $|H^{\text{RT}}(\omega)|$ reaches the local maximum at f_k^{RT} , where

$$f_k^{\text{RT}} = (2k + 1) \frac{v}{4x}, k = 0, 1, 2, \dots \quad (11)$$

When $x = x_f$, we have $f_k^{\text{RT}} = f_k^{\text{DT}}, \forall k \in \mathbb{N}^*$, thus all local maxima of the two transfer functions are superposed, resulting in a maximum energy, while for other GFLs, the mismatch of local maxima makes the magnitude behavior lose harmonic characteristics. Therefore, the effectiveness of EMTR fault location methods seems to be irrelevant to $U(\omega)$ and only results from the magnitude characteristics of the transfer functions. Therefore, it is possible for us to use a given (almost arbitrary) signal in Eq. (5).

III. EMTR-CONV ALGORITHM: MULTI-PHASE TRANSMISSION LINE CASES

A. EMTR-conv in multi-phase transmission lines

The derivation in section II is for single-phase transmission line cases. For multi-phase transmission lines, either a single excitation source or multiple sources on all phases can be adopted in the reverse process (because the excitation sources in the reverse process can be arbitrary), and then different

fault types are assumed and the transients at all GFLs are pre-calculated. When a real fault occurs, the fault type is first recognized by the fault-generated transients, then the fault-generated transient is convoluted with the corresponding pre-stored signals to accomplish the fault location. The maximal CSE corresponds to the real fault position.

The flowchart of EMTR-conv for multi-phase transmission line cases is shown in Table II.

TABLE II. THE EMTR-CONV ALGORITHM FOR MULTI-PHASE TRANSMISSION LINES

Input: network parameters and topology; a given excitation signal $u(t)$ (e.g., a lightning impulse); a measured voltage signal $u_0^{DT}(t)$ generated by a fault
1. Set a series of phase-to-ground, phase-to-phase and 3-phase short-circuit branches along the line as the GFLs respectively.
2. $u(t)$ is injected into the network at a terminal of the line either on a single phase or on all 3 phases. The short-circuit transient $i_f^{RT}(x, t)$ for each GFL is calculated and stored.
3. When the fault occurs, the fault-generated transient signal $u_0^{DT}(t)$ is collected at the same terminal as in step 2.
4. Recognize the fault type according to the waveform and amplitude of the transient.
5. With the knowledge of fault type, do the convolution of $u_0^{DT}(t)$ and the corresponding $i_f^{RT}(x, t)$ of the same fault type, and the result is denoted as $c(x, t)$.
6. Calculate the energy of $c(x, t)$ which is denoted by $E(x)$.
Output: the predicted fault location is $x_f = \arg \max_x (E(x))$.

B. Validation in a 100-km transmission line

Fig. 3 represents for a 100-km 3-phase transmission line. The transmission line parameters are shown in Table III, and the model is implemented in PSCAD/EMTDC. 220-kV sources are applied at the left end of the line and 100-k Ω resistances are used to represent the power transformers at both ends of the line in the transient simulations. Different types of faults are assumed at $x = x_f$ along the line and EMTR-conv are used to locate the faults.

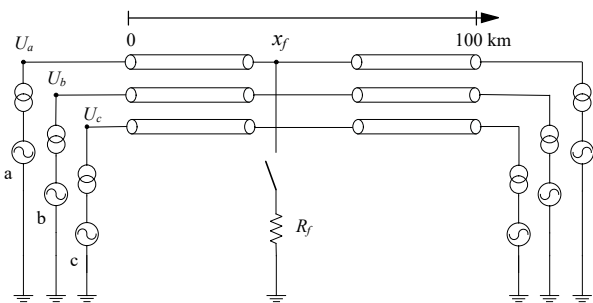


Fig. 3. The schematic representation for a 3-phase transmission line and a phase-to-ground fault. Constant line parameters are shown in the Appendix.

1) Phase-to-ground fault

A Phase-A-to-ground fault that occurs at the angle of 90° is set at $x=30$ km. The fault impedance is 1Ω . The lightning impulse in section II is used as the excitation source in the reverse process, and the excitation signal is injected either only on Phase A or on all 3 phases, then the fault currents at different GFLs are stored. The CSEs are obtained using the convolution of the pre-stored fault currents and the real fault-

generated transient voltage at the head end of the network on Phase A. The CSEs are shown in Fig. 4.

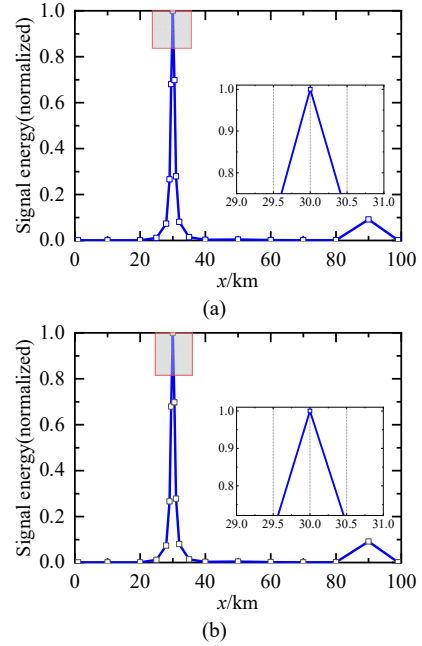


Fig. 4. CSE of a Phase-A-to-ground fault at $x=30$ km for different excitation sources in the reverse process (a) $u(t)$; $u(t)$; $u(t)$, (b) $u(t)$; 0; 0.

Fig. 4 shows different excitation sources in the reverse process have no impact on the accuracy of EMTR-conv method for phase-to-ground faults. This can be understood as follows. Considering the coupling between different phases, the influence of the other two excitation sources from Phase B and C is equivalent to a change of the excitation source on Phase A, thus has no impact on the location result because the excitation source can be arbitrarily selected for EMTR-conv algorithm.

Therefore, in the following examples (that do not take the frequency-dependent parameters into account), for convenience, only one excitation source (i.e., $u(t)$; 0; 0) is injected into the network in the reverse process.

2) Phase-to-Phase fault

Phase-A-to-Phase-B faults are set along the line each separated with a distance of 10 km. The fault angle and impedance remain 90° and 1Ω . The current flowing from phase A to phase B at different GFLs under the excitation source (8) on phase A are pre-calculated, and convoluted with the real fault-generated voltage on phase A during the forward process.

3) 3-Phase fault

3-Phase faults are also set along the line each separated with a distance of 10 km. The fault impedance between each phase is assumed to be 1Ω . The fault angle and excitation source remain 90° and (8) on phase A, respectively.

The current flowing from phase A to phase B at different GFLs are calculated and then convoluted with fault-generated voltage on phase A in the forward process.

TABLE III. FAULT LOCATION RESULTS AND THE ERROR (%) FOR DIFFERENT FAULT TYPES AND FAULT POSITIONS USING EMTR-CONV

x_f/L	P-G (Single)	P-G (Triple)	P-P	3P
0.01	1 (0.00)	1 (0.00)	1 (0.00)	1 (0.00)
0.1	10 (0.00)	10 (0.00)	10 (0.00)	10 (0.00)

0.2	19.99 (0.01)	19.99 (0.01)	20 (0.00)	20 (0.00)
0.3	30 (0.00)	30 (0.00)	30 (0.00)	30 (0.00)
0.4	40 (0.00)	40 (0.00)	40 (0.00)	40 (0.00)
0.5	50 (0.00)	50 (0.00)	49.97 (0.03)	50 (0.00)
0.6	60 (0.00)	60 (0.00)	60 (0.00)	60 (0.00)
0.7	70 (0.00)	70 (0.00)	70 (0.00)	70 (0.00)
0.8	80.01 (0.01)	80 (0.00)	80 (0.00)	80 (0.00)
0.9	90 (0.00)	90 (0.00)	90 (0.00)	90 (0.00)
0.99	99 (0.00)	99 (0.00)	99 (0.00)	99 (0.00)

The CSEs are shown in Table III, where 19.99 (0.01) means the location result is 19.99 km and the error is 0.01%. It can be summarized that for different fault types in multi-phase transmission lines, EMTR-conv method works reliably for frequency-independent line parameters, and reaches an error of less than 0.03%.

IV. EMTR-CONV FOR MULTI-PHASE LINES CONSIDERING FREQUENCY-DEPENDENT PARAMETERS AND LOSSY GROUND

A. Performance of EMTR-conv considering frequency-dependent parameters and lossy ground

The parameters of real transmission lines are frequency-dependent and affected by the lossy ground. In previous studies of EMTR-based methods, the electromagnetic transient signals in the reverse processes are acquired using constant-parameter transmission line models in simulation.

To study the influence of this simplification, in this section the power network topology and fault conditions remain the same in section III, however the transmission line model used in the forward process is replaced by frequency-dependent models, while constant line parameter model is used in the reverse process.

For all 3 fault types and different ground conductivities, EMTR-conv method is used, and the CSEs are shown in Fig. 5 and Fig. 6.

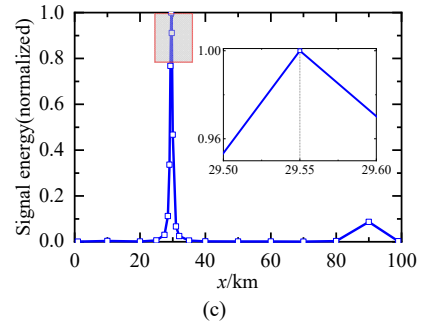
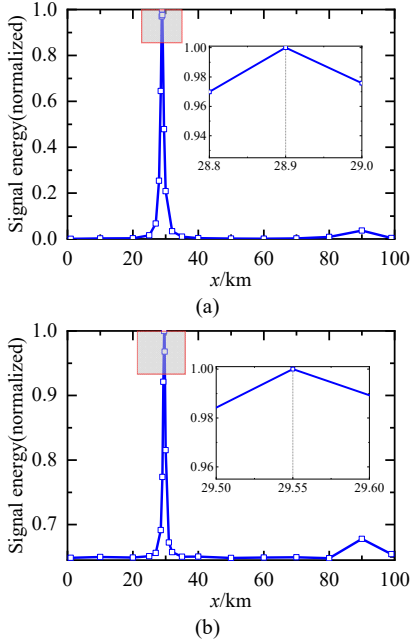


Fig. 5. CSE for (a) Phase-A-to-ground fault, (b) Phase A-to-Phase B fault, (c) 3-Phase fault at $x=30$ km, $\rho_g = 10\Omega \cdot \text{m}$.

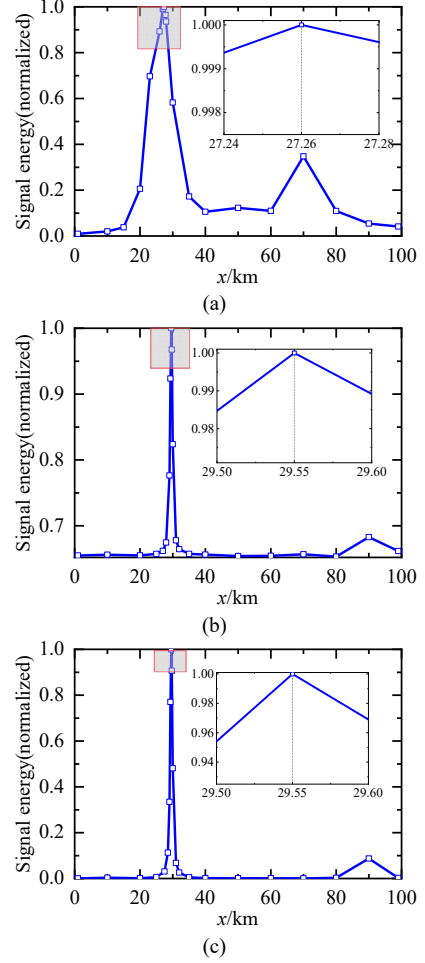


Fig. 6. CSE for (a) Phase A-to-ground fault, (b) Phase A-to-Phase B fault, (c) 3-Phase fault at $x=30$ km, $\rho_g = 1000\Omega \cdot \text{m}$.

As is shown in Figs. 5 and 6, the mismatch of transmission line models in the forward and reverse process has an impact on the location accuracy especially when the soil resistivity is high, for instance, an error of nearly 9% for phase-to-ground faults when the ground resistivity is $1000 \Omega \cdot \text{m}$.

For a lossy transmission line, dissipation of the transient signal energy (SE) occurs during its propagation and grows as the distance increases. Therefore, the SE at $x=x_f$ (the real fault position) decreases more than those at $x < x_f$, therefore the location result may be slightly ahead of the real fault position.

In addition, Fig. 7 shows the relationship between location error and the fault position x_f , which is approximately proportional. For P-P and 3P faults, the location error is

almost unaffected by the ground conductivity since the ground mode is not involved in the fault current path; while for P-G faults, the location error grows as the ground resistivity increases, and the rough proportion relationship in Fig. 7(a) also deteriorates accordingly but still holds satisfied.

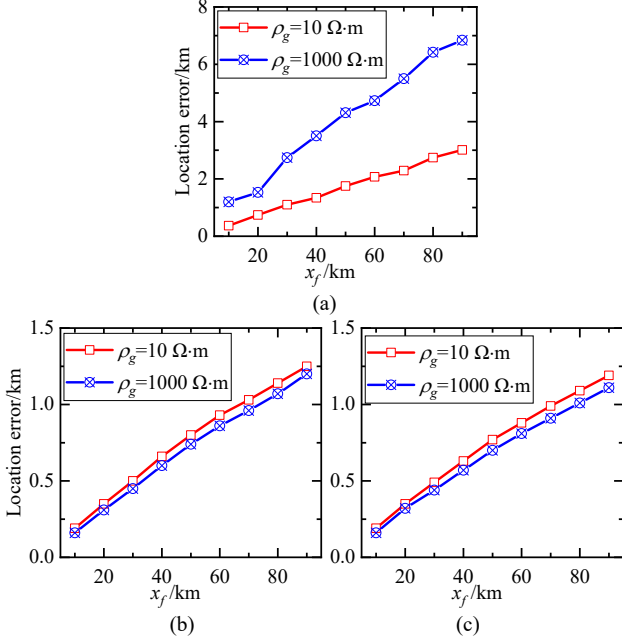


Fig. 7. The location error of (a) phase-to-ground fault, (b) phase-to-phase fault and (c) 3-phase fault as a function of real fault position.

B. Correction to EMTR-conv using double observation points

According to Fig. 7, it is reasonable to assume the location error

$$\Delta x_f = x_f - x = \lambda x_f, \quad (12)$$

Where Δx_f is the location error, x_f is the real fault position and x is the preliminary location result acquired using EMTR-conv. λ is a parameter that represents the linear relationship.

If we set two observation points OB1 and OB2 at the ends of the line with a length of L , and use EMTR-conv to locate a fault respectively. The maximum points of FCSEs (also the preliminary location results) are x_1 and x_2 , we have

$$\begin{aligned} x_f - x_1 &= \lambda x_f \\ x_2 - x_f &= \lambda (L - x_f) \end{aligned} \quad (13)$$

According to (13), the real fault position is

$$x_f = \frac{Lx_1}{L + x_1 - x_2}. \quad (14)$$

Therefore, the fault location result can be corrected by using dual observation points and performing the EMTR-conv method twice, as is shown in Eq. (14).

Noting that $x_1 \approx x_2$, the denominator of (14) will not be zero, therefore (14) always works.

We wish to emphasize that the method described by Eqs (13) and (14) can also be used for other EMTR-based fault location methods provided that their location errors grow roughly linearly as the distance increases.

C. Discussion

The correction formula (14) relies on the linear relationship between the error and distance. We now give a brief analysis.

As shown in Eqs. (10) and (11), when $x = x_f$, we have $f_k^{\text{RT}} = f_k^{\text{DT}}$, thus all local maxima of the two transfer functions are superposed.

However, considering frequency-dependent parameters, the velocity becomes frequency-dependent as $v=v(f)$, which is shown in Fig. 8 for a single-conductor line with a height of 10 m and wire diameter of 1 cm. From Fig. 8, the relationship is approximately logarithmic, namely,

$$v(f) = v_c \ln \frac{f}{f_0} + v(f_0). \quad (15)$$

where v_c is a fitting coefficient.

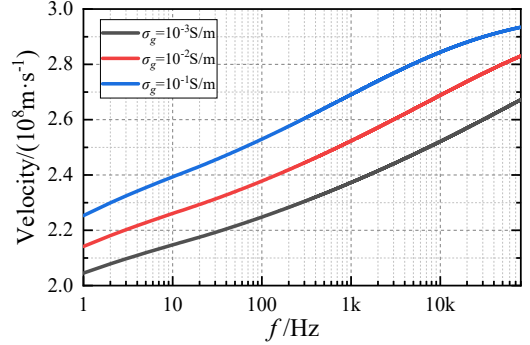


Fig. 8. Wave velocity for different ground conductivities. The wire conductivity is $5.8 \times 10^7 \text{ S/m}$ and the ground relative permittivity equals to 10.

The magnitude of the transfer functions in the forward process for frequency-dependent and frequency-independent parameters reaches the local maximums at a series of frequencies $f_k^{\text{DT,FD}}$ and $f_k^{\text{DT,FI}}$, respectively,

$$f_k^{\text{DT,FD}} = (2k+1) \frac{v(f_k^{\text{DT,FD}})}{4x_f}, k = 0, 1, 2, \dots \quad (16)$$

$$f_k^{\text{DT,FI}} = (2k+1) \frac{v^{\text{FI}}}{4x_f}, k = 0, 1, 2, \dots$$

where FD and FI are the abbreviations of frequency-dependent and frequency-independent respectively, and v^{FI} is the velocity for constant-parameter lines.

Note that $f_k^{\text{DT,FD}} \approx f_k^{\text{DT,FI}}$, by Taylor's expansion,

$$v(f_k^{\text{DT,FD}}) \approx v(f_k^{\text{DT,FI}}) + \frac{v_c}{f_k^{\text{DT,FI}}} (f_k^{\text{DT,FD}} - f_k^{\text{DT,FI}}). \quad (17)$$

For each k , let $f_k^{\text{RT}} = f_k^{\text{DT,FD}}$, we will have a series of preliminary location results x_k under each given frequency $f_k^{\text{DT,FD}}$, and the corresponding λ_k defined in Eq. (12) can be estimated using (15)-(17),

$$\lambda_k = \frac{v(f_k^{\text{DT,FI}}) - v^{\text{FI}}}{v(f_k^{\text{DT,FI}}) - v_c}, k = 0, 1, 2, \dots, \quad (18)$$

As shown in Table IV, most of the energy (more than 95%) concentrates on a frequency spectrum of $[0, 20f_0^{\text{DT,FD}}]$, therefore, thus only $k < 10$ needs to be considered among all λ_k . Fig. 9 shows different λ_k calculated by Eq. (18) and the

real λ acquired by EMTR-conv method where the maximal difference is less than 8%, and the real λ is very close to that of λ_0 . Therefore, it is reasonable to regard it as a constant at all positions along the line and the location error grows with the distance roughly linearly.

TABLE IV. ENERGY RATIO OF $H^{DT}(\omega)$ WITH DIFFERENT FREQUENCY RANGE

x_f/km	$f/f_0^{\text{DT,FD}}$			
	10	15	20	25
10	0.852	0.919	0.955	0.975
20	0.856	0.922	0.957	0.976
50	0.858	0.924	0.958	0.977
100	0.858	0.924	0.959	0.978
500	0.854	0.920	0.957	0.977

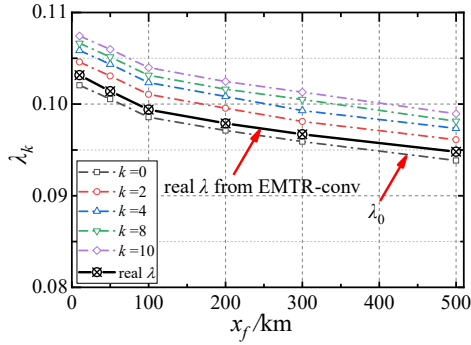


Fig. 9. The coefficient λ_k acquired using equation (18). The black solid line represents the real λ acquired from EMTR-conv method.

V. APPLICATION EXAMPLES

Numerical experiments are carried out in a 220-kV, 300-km 3-phase transmission line. The tower structure and line models are shown in Fig. 10 [20] and Table V.

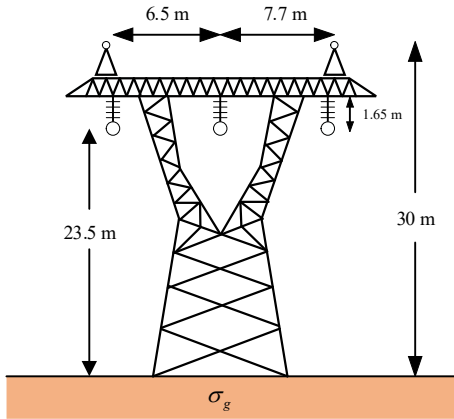


Fig. 10. Tower structure for a 220-kV 3-phase transmission line with 2 ground wires. σ_g is the ground conductivity.

TABLE V. LINE PARAMETERS

Parameter	Value
Conductor	2*LGI-400/35
Ground wire	JLB4-150
Sag	11 m

As shown in Fig. 7 and Fig. 8, the influence of the frequency-dependent parameters is more obvious when the

ground resistivity is high. Therefore, for all fault types, the ground resistivity is assumed to be $1000 \Omega \cdot \text{m}$. The P-G fault impedances are set to be 10Ω , while the P-P and 3P fault impedances are assumed to be 1Ω . The location errors of the EMTR-conv without and with correction are shown in Fig. 11, which indicates the error can be greatly reduced (e.g., 200 m on average for P-G faults after correction) using the correction defined by Eq. (14).

In addition, the results of travelling wave-based fault location method using Time Difference of Arrival (TDOA) is provided for comparison. Classical two-end metric which requires time synchronization is used, as shown in Eq. (19) and Fig. 11. The sampling rate is 1 MS/s, the same as EMTR-conv method.

$$x_{f,\text{TDOA}} = 0.5 \cdot (L - v \cdot (t_L - t_0)). \quad (19)$$

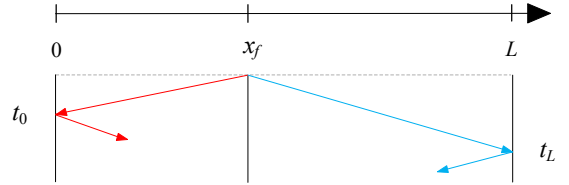


Fig. 11. Lattice diagram of fault-generated traveling waves measured for TDOA at the two terminals.

The results in Fig. 12 show that EMTR-conv corrected by double OB performs better, and works reliably even for 300-km transmission lines.

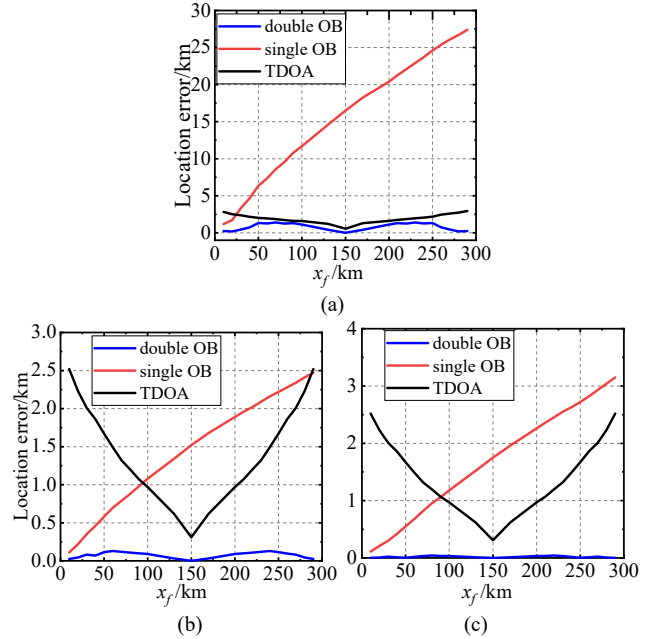


Fig. 12. The location error of (a) phase-to-ground fault, (b) phase-to-phase fault and (c) 3-phase fault as a function of real fault position, $\rho_g = 1000 \Omega \cdot \text{m}$. Here double OB means EMTR-conv with correction of (10), Single OB means EMTR-conv without correction.

A. Influence of ground conductivity

For phase-to-phase and 3-phase faults, the ground is not involved in the fault current path, therefore the location accuracy is not sensitive to the ground conductivity. Therefore, only phase -to-ground faults under different ground resistivities are considered in this section, and the results are shown in Fig. 13. The fault impedance remains 10Ω and the fault angle is 90° .

TABLE VI. FAULT LOCATION ERROR FOR DIFFERENT FAULT TYPES, FAULT POSITIONS, INCEPTION ANGLES AND FAULT IMPEDANCE

x_f /km	Location error in meters							
	P-G/ 5°/10 Ω	P-G/ 90°/10 Ω	P-G/ 90°/1 Ω	P-G/ 90°/100 Ω	P-P/ 5°/1 Ω	P-P/ 90°/1 Ω	3P/ 5°/1 Ω	3P/ 90°/1 Ω
30	531(1.77‰)	531(1.77‰)	449(1.50‰)	786(2.62‰)	81(0.27‰)	81(0.27‰)	23(0.08‰)	23(0.08‰)
50	1667(5.56‰)	1667(5.56‰)	1329(4.43‰)	2003(6.68‰)	114(0.38‰)	114(0.38‰)	5(0.02‰)	5(0.02‰)
70	1538(5.13‰)	1538(5.13‰)	1397(4.66‰)	2024(6.75‰)	119(0.40‰)	119(0.40‰)	34(0.11‰)	34(0.11‰)
100	1299(4.33‰)	1299(4.33‰)	1120(3.73‰)	1857(6.19‰)	91(0.30‰)	91(0.30‰)	34(0.11‰)	34(0.11‰)
130	782(2.61‰)	782(2.61‰)	410(1.37‰)	930(3.10‰)	32(0.11‰)	32(0.11‰)	12(0.04‰)	12(0.04‰)
150	0(0)	0(0)	0(0)	82(0.27‰)	0(0)	0(0)	0(0)	0(0)
170	782(2.61‰)	782(2.61‰)	410(1.37‰)	932(3.11‰)	32(0.11‰)	32(0.11‰)	12(0.04‰)	12(0.04‰)
200	1299(4.33‰)	1299(4.33‰)	1120(3.73‰)	1860(6.20‰)	91(0.30‰)	91(0.30‰)	34(0.11‰)	34(0.11‰)
230	1538(5.13‰)	1538(5.13‰)	1397(4.66‰)	2028(6.76‰)	119(0.40‰)	119(0.40‰)	34(0.11‰)	34(0.11‰)
250	1667(5.56‰)	1667(5.56‰)	1329(4.43‰)	2004(6.68‰)	114(0.38‰)	114(0.38‰)	5(0.02‰)	5(0.02‰)
270	531(1.77‰)	531(1.77‰)	449(1.50‰)	791(2.64‰)	81(0.27‰)	81(0.27‰)	23(0.08‰)	23(0.08‰)
290	292(0.97‰)	292(0.97‰)	241(0.80‰)	405(1.35‰)	24(0.08‰)	24(0.08‰)	1(0.003‰)	1(0.003‰)

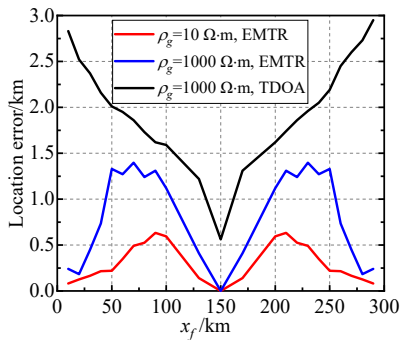


Fig. 13. The location error for P-G fault with different ground resistivity at different fault positions. Line length is 100 km. EMTR means EMTR-conv with correction Eq. (10).

According to Eq. (8) and (9), the performance of EMTR-conv using double OB correction relies on the proportional relationship between location error and fault distance. As shown in Fig. 9(a), when the ground resistivity increase, this linear relationship is worse than that of the lower ground resistivity. Therefore, the location accuracy decreases when the ground resistivity is high, although still better than TDOA as shown in Fig. 13.

It is interesting to observe that the location errors shown in Fig. 13 has a minimum near the two ends and the middle of the line. Due to the loss and frequency-dependency, we can infer that the two preliminary location results satisfy $x_1 \leq x_f \leq x_2$. If the fault occurs at $x_f = 0$, then $x_1 = 0$ and ideally, the final result $x^* = 0$, which is exact. For the fault at the middle, by symmetry $x_1 + x_2 = 2x_f = L$, again resulting in an error of 0. Therefore, we may infer that the location results for $x_f = 0, 0.5L$ and L have no error in theory. Consequently, the fault location errors close to the terminals will be small, which is different from TDOA-based methods.

B. Influence of fault angle

Fault angle affects the amplitude of the fault-generated transient, therefore it may have an influence on the location accuracy.

Many different faults occurring between 10 km to 290 km are assumed, and then located using double observation points. The ground resistivity and fault impedance remain 1000 $\Omega \cdot m$ and 10 Ω . The fault angle is assumed to be 5°, 30° and 90° respectively.

The average and distribution ranges of the location errors under different fault angles are shown in Table VI, which suggests the method is insensitive to the fault angles, or alternatively the amplitude of fault-generated transients.

C. Influence of fault impedance

Different fault impedances affect the wave propagation, therefore change the characteristics of the transient waveform. The fault impedances for P-P and 3P faults may not be very large in general. Therefore, only P-G faults are tested to estimate the influence.

As is discussed in [24][25], the classical EMTR-based fault location methods may become invalid for very high-impedances (i.e., above 300 Ω) faults. Therefore, fault impedances of 1, 10 and 100 Ω are used to estimate the error of EMTR-conv using double observation points. The ground resistivity and fault angle remain 1000 $\Omega \cdot m$ and 90° respectively.

Table VI shows that the average of the location errors is slightly higher for the faults with a higher impedance, because the waveform not only decays but also deforms.

However, the location error can still be greatly reduced (to less than 7‰) using double observation points. It is likely that the method may give different location results for a fault at the same point due to different fault impedances or angles. However, the derivation of Eq. (18) shows λ_k does not depend on these parameters, but only on the transfer functions. So we can expect the correction equation is still applicable.

VI. CONCLUSION

We briefly reviewed the EMTR-based fault location method using direct convolution (EMTR-conv), and extended the method to multi-phase transmission lines.

Noting that the parameters of real transmission lines are frequency-dependent and affected by lossy ground, while

constant parameters are often used during the reverse process in EMTR-based fault location methods, this consistency may greatly degrade the location accuracy. Therefore, we investigated the performance of EMTR-based fault location methods (using EMTR-conv as an example) using frequency-dependent transmission line models in the forward process but constant parameters in the reverse process, and find that the location error is approximately proportional to the fault distance.

Based on this observation, we propose a correction method using double observation points at both ends of the line to overcome the problem. We can use the transient data at the end of the line to perform EMTR-conv respectively to locate the fault preliminarily, and then correct the preliminary location results based on the assumption that the location error is approximately proportional to the fault distance. The location error is then greatly reduced.

Numerical experiments are carried out in a 220-kV 300-km transmission line considering frequency-dependent parameters and different fault conditions. The results show that the location errors using the correction proposed in this paper can be greatly reduced for long transmission lines.

The horizontal non-homogeneities of the ground resistivity will affect the wave velocity, and its complex influence will be analyzed in future.

APPENDIX

PARAMETERS OF THE TRANSMISSION LINE PRESENTED IN FIG.3

The series impedance and shunt admittance matrices at 50 Hz for the 3-phase transmission line shown in Fig. 3 are given by equation (20) and (21).

$$Z = \begin{bmatrix} 0.081 + j0.696 & 0.047 + j0.309 & 0.047 + j0.309 \\ 0.047 + j0.309 & 0.081 + j0.696 & 0.047 + j0.309 \\ 0.047 + j0.309 & 0.047 + j0.309 & 0.081 + j0.696 \end{bmatrix} \frac{\Omega}{\text{km}} \quad (20)$$

$$Y = \begin{bmatrix} 10^{-2} + j2.48 & -j0.48 & -j0.48 \\ -j0.48 & 10^{-2} + j2.48 & -j0.48 \\ -j0.48 & -j0.48 & 10^{-2} + j2.48 \end{bmatrix} \frac{\mu\text{S}}{\text{km}} \quad (21)$$

REFERENCES

- [1] Kawady T, Stenzel J. A practical fault location approach for double circuit transmission lines using single end data. *IEEE Transactions on Power Delivery*, 2003, 18(4): 1166-1173.
- [2] Liao Y. Fault location for single-circuit line based on bus-impedance matrix utilizing voltage measurements. *IEEE Transactions on Power Delivery*, 2008, 23(2): 609-617.
- [3] Gale P, Crossley P, Bingyin X, et al. Fault location based on travelling waves. 1993 Fifth International Conference on Developments in Power System Protection, 1993: 54-59.
- [4] Magnago F H, Abur A. Fault location using wavelets. *IEEE Transactions on Power Delivery*, 1998, 13(4): 1475-1480.
- [5] Hamidi R J, Livani H. Traveling-wave-based fault-location algorithm for hybrid multiterminal circuits. *IEEE Transactions on Power Delivery*, 2016, 32(1): 135-144.
- [6] OD Naidu, and Ashok Kumar Pradhan. A Traveling Wave-Based Fault Location Method Using Unsynchronized Current Measurements. *IEEE Transactions on Power Delivery*, 2019, 34(2): 505-513.
- [7] Mahmoudimanesh H, Lugrin G, Razzaghi R, et al. A new method to locate faults in power networks based on electromagnetic time reversal. 13th IEEE Signal Processing Advances in Wireless Communications (SPAWC), 2012: 469-474.
- [8] Razzaghi R, Lugrin G, Manesh H M, et al. An Efficient Method Based on the Electromagnetic Time Reversal to Locate Faults in Power Networks[J]. *IEEE Transactions on Power Delivery*, 2013, 28(3):1663-1673.
- [9] Razzaghi R, Lugrin G, Rachidi F, et al. Assessment of the influence of losses on the performance of the electromagnetic time reversal fault location method. *IEEE Transactions on Power Delivery*, 2017, 32(5): 2303-2312.
- [10] Rachidi F, Rubinstein M, Paolone M. *Electromagnetic time reversal: Application to EMC and power systems*. John Wiley & Sons, 2017.
- [11] J. Sun, Q. Yang, W. Xu and W. He, "A Distribution Line Fault Location Estimation Algorithm Based on Electromagnetic Time-Reversal Method Calculated in the Finite Difference Time Domain," *IEEE Transactions on Electromagnetic Compatibility*, vol. 64, no. 3, pp. 865-873, June 2022
- [12] Wang Z, He S, Li Q, et al. A full-Scale experimental validation of electromagnetic time reversal applied to locate disturbances in overhead power distribution lines. *IEEE Transactions on Electromagnetic Compatibility*, 2018, 60(5): 1562-1570.
- [13] Zhaoyang Wang, Reza Razzaghi, Mario Paolone, Farhad Rachidi. Time reversal applied to fault location in power networks: Pilot test results and analyses. *Electrical Power and Energy Systems* 114 (2020) 105382.
- [14] Redy Mardiana, Haifa Al Motairy, and Charles Q. Su. Ground Fault Location on a Transmission Line Using High-Frequency Transient Voltages. *IEEE Transactions on Power Delivery*, 2011, 26(2): 1298-1299.
- [15] Jing Ma, Yuxin Shi, Wei Ma, and Zengping Wang, Location Method for Interline and Grounded Faults of Double-Circuit Transmission Lines Based on Distributed Parameters. *IEEE Transactions on Power Delivery*, 2015, 30(3): 1307-1316.
- [16] Yu-Ju Lee , Ching-Hsin Chao, Tzu-Chiao Lin , and Chih-Wen Liu. A Synchrophasor-Based Fault Location Method for Three-Terminal Hybrid Transmission Lines With One Off-Service Line Branch. *IEEE Transactions on Power Delivery*, 2018, 33(6): 3249-3251.
- [17] Yachao Yang , Chun Huang , and Qianming Xu. A Fault Location Method Suitable for Low-Voltage DC Line. *IEEE Transactions on Power Delivery*, 2020, 35(1): 194-204.
- [18] G. Wang and C. Zhuang, "A Fault Location Method Using Direct Convolution: Electromagnetic Time Reversal or Not Reversal," in *IEEE Transactions on Electromagnetic Compatibility*, doi: 10.1109/TEM.2022.3168012.
- [19] Z. Wang, R. Razzaghi, M. Paolone and F. Rachidi, Electromagnetic Time Reversal Similarity Characteristics and Its Application to Locating Faults in Power Networks, *IEEE Transactions on Power Delivery*, vol. 35, no. 4, pp. 1735-1748, Aug. 2020.
- [20] Banjanin, Mladen S. Application possibilities of special lightning protection systems of overhead distribution and transmission lines[J]. *International Journal of Electrical Power & Energy Systems*, 2018, 100:482-488.
- [21] J. R. Carson. Wave propagation in overhead wires with ground return. *Bell System Technical Journal*, 1926, 5: 539-554.
- [22] R. G. Olsen, T. A. Pankaskie. On the exact, Carson and image theories for wires at or above the earth's interface. *IEEE Transactions on Power Apparatus and Systems*, 1983, 102(4): 769-778.
- [23] C. R. Paul. *Analysis of multiconductor transmission lines*. New York: John Wiley & Sons Press, 2008.
- [24] Jianwei An, Chijie Zhuang, Farhad Rachidi, Rong Zeng. An effective EMTR-based high-impedance fault location method for transmission lines. *IEEE Transactions on Electromagnetic Compatibility*. 2021, 63(1): 268-276.
- [25] J. Sun, Q. Yang, H. Cui, J. Ran and H. Liu, "Distribution Line Fault Location With Unknown Fault Impedance Based on Electromagnetic Time Reversal," in *IEEE Transactions on Electromagnetic Compatibility*, doi: 10.1109/TEM.2021.3097105.
- [26] B. Bogert. Demonstration of Delay Distortion Correction by Time-Reversal Techniques. *IRE Transactions on Communications Systems*, 1957,5(3):2-7.
- [27] Q. Li, Z. Wang, Y. -Z. Xie, F. Rachidi and M. Rubinstein, "A Correlation-Based Electromagnetic Time Reversal Technique to

Locate Indoor Transient Radiation Sources," IEEE Transactions on Microwave Theory and Techniques, vol. 69, no. 9, 3945-3957, 2021.

- [28] Z. Wang, F. Rachidi, M. Paolone, M. Rubinstein and R. Razzaghi, "A Closed Time-Reversal Cavity for Electromagnetic Waves in Transmission Line Networks," in IEEE Transactions on Antennas and Propagation, vol. 69, no. 3, pp. 1621-1630, March 2021.
- [29] Wang Z, Codino A, Razzaghi R, et al. Using electromagnetic time reversal to locate faults in transmission lines: Definition and application of the mirrored minimum energy property. Int. Symp. Electromagn. Compat.(EMC Europe), Angers, France, 2017: 1-6.